# An Integrated Magnetic Structure for Bi-Directional Two-Channel Interleaved Boost Converter with Coupled Inductor

Abdul Basit Mirza, Asif Imran Emon, Sama Salehi Vala and Fang Luo
Department of Electrical and Computer Engineering
Stony Brook University
Stony Brook, NY, United States
abdulbasit.mirza@stonybrook.edu

Abstract— The channel current in an interleaved boost converter consists of circulating Differential Mode (DM) current and Common Mode (CM) boost current. Inversecoupling between inductors, compared with the uncoupled case, offers reduced channel current ripple. However, its leakage inductance, that serves as boost inductor, is difficult to control. Hence, a cascade of two perfectly coupled inductors, inverse (DM inductance) and direct (CM inductance), is preferred. The DM and CM currents and their ripples depend on these inductances. Nonetheless, this approach results in increased size of magnetics. In this paper, an integrated inductor, based on gapped EE-core is proposed, that combines both CM and DM inductances in a single core. The CM and DM inductances are independent and can be controlled separately by their winding turns. A reluctance model is derived, and a design procedure is developed where core parameters are expressed in terms of converter parameters. Finally, the proposed concept is validated through a 330W, 100 V to 168 V prototype.

Keywords— Interleaved Boost Converter, Integrated Magnetic Structure, EE-core, Coupled Inductor, CM and DM inductance.

# I. INTRODUCTION

Two-phase interleaving in a simple boost converter has benefits like twice effective switching frequency, harmonic cancellation; better efficiency and increased power density [1]. It is also beneficial for the output filter capacitor. The Equivalent Series Resistance (ESR) of tantalum capacitor is inversely proportional to the frequency of the switching current and interleaving can effectively reduce the filter capacitor size, loss and weight [2]. Further due to phase shift between the channel currents, the input current ripple is also lower compared with the non-interleaved case. However, the lower input current ripple is achieved through ripple cancellation of the channel ripples, the channel or inductor current ripple is still large if small inductance is used.

Inverse coupling between channel inductors is proved to be effective in lowering the channel current ripple while maintaining same input current ripple [1]. Fig. 1 shows a two-phase interleaved boost converter with inverse coupled inductor. Inverse coupling results in different equivalent inductances for different modes of operation. The equivalent inductances are dependent on the duty ratio and the self and mutual inductances L and M.

Further, an usual phenomenon associated with interleaving is the circulating DM current  $i_{DM}(t)$  that flows between the channels. This circulating current is an inherent feature of interleaving regardless of coupling between the channels. The circulating current flows on top of the boost current  $i_{CM}(t)$ , which is CM as it flows in same direction in

both channels. Fig. 1 shows the direction of the  $i_{CM}(t)$  and  $i_{DM}(t)$ . For inverse coupled case, the DM current  $i_{DM}(t)$  is dependent on mutual inductance M and is generated by the differential voltage, which is produced due to switching of lower switches  $S_1$  and  $S_2$ . The CM current  $i_{CM}(t)$  is dependent on the leakage inductance L-M of the inverse coupled inductor. Nonetheless, the desired value of boost inductance L - M is difficult to achieve as it depends on the layout of the winding and the structure of the core. To mitigate this issue, inverse coupled inductor can be realized through cascade of two separate perfectly inverse  $(L_{DM})$  and direct  $(L_{CM})$  coupled inductors as proposed in [2] and [3]. Fig. 2 shows the transformation. Based on the direction of coupling,  $i_{CM}(t)$  only sees  $L_{CM}$  and  $i_{DM}(t)$  only sees  $L_{DM}$ . This implementation allows desired value of boost inductance to be realized and to reap the benefit of inverse coupling, which is to reduce the channel current ripple while maintaining the same transient response.

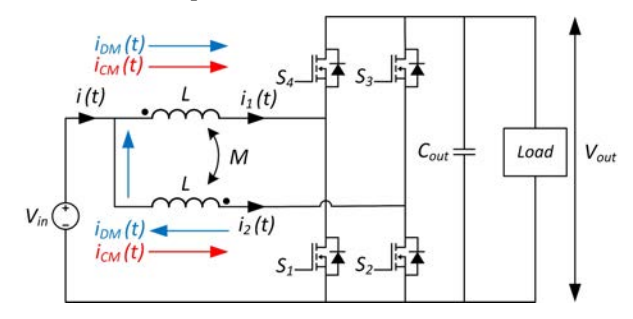


Fig. 1. Two-phase interleaved boost converter with inverse coupled inductor.

The inverse and direct coupled inductor implementation of inverse coupled inductor requires two separate cores, which increases the overall size of magnetics. Several approaches have been proposed for miniaturization of magnetics by integrating both  $L_{CM}$  and  $L_{DM}$  in a single structure. An EIE core based integrated structure is proposed in [4]. The structure utilizes two airgaps for energy storage, it is shown that the total airgap length required is less than for EE-core structure; however, a detailed comparison is not provided. Further, the inductances  $L_{CM}$  and  $L_{DM}$  are not independent and cannot be controlled separately. A CCTT-core based magnetic structure is proved in [5] to reduce the effect of fringe loss in the windings. The associated near-field emission is also less compared with the EE structure. However, the structure requires custom designed cores, which increases the cost of the design. Also, the CM and DM inductances are also not decoupled as in [4]. Decoupling between CM and DM inductances can be achieved by through a structure shown in Fig. 2 in [6]. The inductances are built on the two outer legs of the core. In contrast to other structures, the airgap is provided on the outer legs instead on the center leg. The structure also exhibits better transient performance. However, the E and I cores needs to be adjusted precisely. The two cores connect with each other through the center leg. Hence, gap filling inside airgaps is necessary to ensure mechanical stability and to prevent displacement between the two cores.

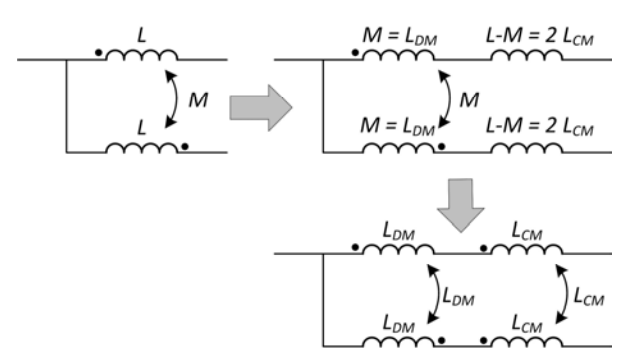


Fig. 2. Transformation of an inverse coupled inductor into inverse and direct coupled inductor.

The concept of integrating CM and DM inductances in a single structure for an interleaved boost converter is analogous to the structure of integrated filter for Electromagnetic Interference (EMI) suppression in power converters. In context of EMI, several structures have been proposed to combine  $L_{CM}$  and  $L_{DM}$ . An integration method using two toroidal cores is proposed in [7]. While the volume is reduced considerably,  $L_{CM}$  and  $L_{DM}$  are not independent and the structure suffers uneven thermal distribution. The stacked toroidal structure in [8] provides, high DM inductance but the size is considerably large. Similarly, the first structure presented in [9] has high-near field emission and  $L_{CM}$  and  $L_{DM}$  are dependent.

The third structure presented in [9] and in [10] propose a design in which  $L_{CM}$  and  $L_{DM}$  depends on different winding turns. Also, it is concluded in [9] that this structure has lower near-field emission along due to near magnetic field cancellation. This paper extends this magnetic design for interleaved boost converter. At first, a brief analysis of interleaved boost converter is presented followed by discussion of the proposed integrated magnetic structure. Later, a reluctance model is derived along with the design procedure. The core parameters are expressed in terms of converter parameters to simplify the design. Lastly, the effectiveness of the proposed structure is validated on a hardware prototype.

# II. CONVERTER DESIGN AND OPERATION

The steady state waveforms of a two-phase interleaved boost converter with perfectly inverse and direct coupled inductor are shown in Fig. 3. For both duty cycle D < 0.5 and D > 0.5, there are four different operating states and the switches ON in these states are shown in the top of the Fig. 3. The CM and DM currents  $i_{CM}(t)$  and  $i_{DM}(t)$  can be expressed in terms of channel currents  $i_1(t)$  and  $i_2(t)$  as:

$$i_{CM}(t) = \frac{i_1(t) + i_2(t)}{2}$$
 (1)

$$i_{DM}(t) = \frac{i_1(t) - i_2(t)}{2}$$
 (2)

The input current can be expressed as  $i(t) = 2i_{CM}(t)$ . Similarly, the ripple in  $i_{CM}(t)$  and  $i_{DM}(t)$ ,  $\Delta i_{CM}$  and  $\Delta i_{DM}$  are related to input current ripple and channel current ripple as:  $\Delta i_{CM} = 0.5\Delta i$  and  $\Delta i_{DM} = \Delta i_1 - \Delta i_{CM} = \Delta i_2 - \Delta i_{CM}$ . Through analysis of the steady-state waveforms, following equations are obtained for  $\Delta i$ ,  $\Delta i_1 = \Delta i_2$  and  $\Delta i_{DM}$  for both D < 0.5 and D > 0.5.

A. D < 0.5

$$\Delta i = \frac{V_{in}D(1-2D)}{2(1-D)fL_{CM}}$$
 (3)

$$\Delta i_1 = \Delta i_2 = \frac{V_{in}D(L_{DM}(1-2D) + L_{CM})}{4L_{CM}L_{DM}(1-D)f}$$
(4)

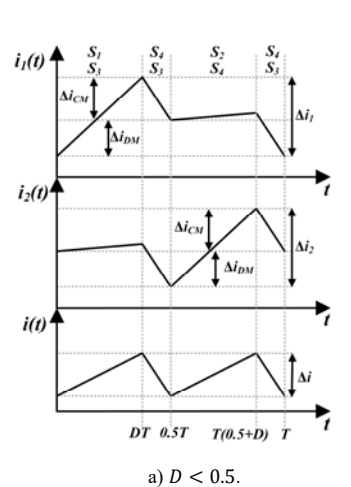
$$\Delta i_{DM} = \frac{V_{in}D}{4L_{DM}(1-D)f} \tag{5}$$

B. D > 0.5

$$\Delta i = \frac{V_{in}(2D-1)}{2fL_{CM}} \tag{6}$$

$$\Delta i_1 = \Delta i_2 = \frac{V_{in}(L_{DM}(1 - 2D) + L_{CM})}{4L_{CM}L_{DM}f}$$
 (7)

$$\Delta i_{DM} = \frac{V_{in}}{4L_{DM}f} \tag{8}$$



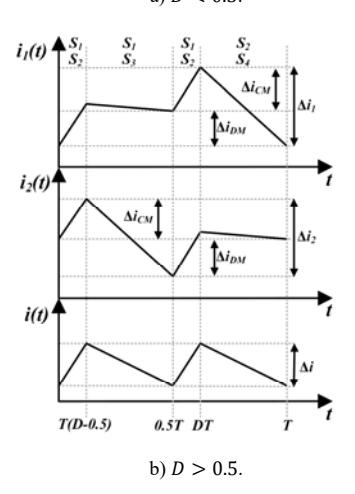
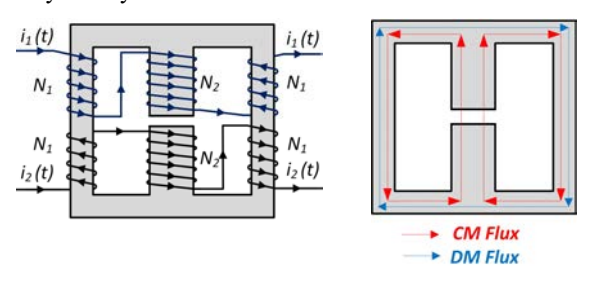


Fig. 3. Steady state waveforms of the converter with perfectly inverse and direct coupled inductor.

### III. INTEGRATED MAGNETIC STRUCTURE

The inverse and direct-coupled implementation of the main inverse coupled inductor in Fig. 2 decouples the CM and DM inductances. With  $L_{CM}$  and  $L_{DM}$  decoupled, desired value of channel current ripple  $\Delta i_1 = \Delta i_2$  and input current ripple  $\Delta i$  can be achieved. However, this implementation results in increased size and volume of magnetics and calls for integration of both inductances in a single structure.

The third EE-core structure for EMI filter with airgap in the middle leg presented in [9] and in [10] decouples  $L_{CM}$  and  $L_{DM}$ . The structure also has lower near-field emission due to near magnetic field cancellation and  $L_{CM}$  is much greater than  $L_{DM}$  due to low reluctance in CM flux path. According to [3] in an interleaved boost converter,  $L_{DM}$  is considerably greater than  $L_{CM}$  [3]. The structure can be extended to inverse and direct-coupled structure (Fig. 2) to achieve miniaturization of magnetics for two-phase interleaved boost converter by interchanging the CM and DM flux paths (Fig. 4). This results in a large value of  $L_{DM}$ . Fig. 4 b) illustrates the flux distribution of CM and DM fluxes; the CM flux has a high reluctance airgap in its path to prevent core saturation. The DM flux path has low reluctance and its direction alternates every half cycle.



a) Winding layout.

b) Flux distribution.

Fig. 4. Proposed integrated magnetic structure for two-phase interleaved boost converter with coupled inductor.

The expressions for  $L_{CM}$  and  $L_{DM}$  can be derived by solving the magnetic equivalent circuits in Fig. 5.  $R_O$  and  $R_C$  are reluctances of half-outer core and center leg including airgap. The center leg windings with  $N_2$  turns are responsible for the CM inductance as the flux produced by the CM current in the center leg is in the same direction. The flux produced by the side limb windings with  $N_1$  turns due to CM currents gets cancelled. On the other hand, the side limb windings with  $N_1$  turns are responsible for DM inductance as the flux produced by DM current gets added, while the flux produced by the center leg windings with  $N_2$  turns gets cancelled. This leads to decoupling between  $L_{CM}$  and  $L_{DM}$  and these inductances depend on separate winding turns  $N_1$  and  $N_2$  respectively.

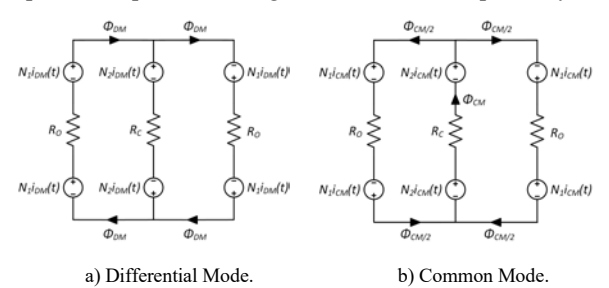


Fig. 5. Magnetic equivalent circuits for the proposed structure.

$$L_{DM} = \frac{2N_1^2}{R_O} \tag{7}$$

$$L_{CM} = \frac{N_2^2}{\frac{R_O}{2} + R_C} \tag{8}$$

# IV. INDUCTOR DESIGN

The design of the proposed structure involves finding the number of turns  $N_1$  and  $N_2$ , while ensuring that the core remains unsaturated. The DM inductance depends on the reluctance of the outer core, which is a known parameter. Hence, for a desired value of  $L_{DM}$ , the required number of turns  $N_1$  can be computed from (7). The number of turns  $N_2$  needs to be chosen such that the core does not get saturated. As evident in Fig. 4 b), the core can saturate in the limb where both CM and DM fluxes add. The maximum value of flux  $\Phi_{Lmax} = B_{Lmax}A_0$  in limb of the core must satisfy the following criteria:  $\Phi_{Lmax} < B_{Sat}A_0$  or  $B_{Lmax} < B_{Sat}$ , where  $A_0$  is the cross sectional area of the limb [11]. The maximum flux  $\Phi_{Lmax}$  comprises of two parts: CM and DM:

$$\Phi_{Lmax} = \Phi_{CMmax} + \Phi_{DMmax} \tag{9}$$

$$\Phi_{CMmax} = \frac{N_2(I_{CM} + 0.5\Delta i_{CM})}{R_c + 0.5 R_O}$$
 (10)

$$\Phi_{DMmax} = \frac{N_1 \Delta i_{DM}}{2R_O} \tag{11}$$

Hence to prevent the core from going into saturation, the following inequality must satisfy:

$$\Phi_{Lmax} < B_{Sat} A_{O}$$

$$\left(\frac{N_{1} \Delta i_{DM}}{2R_{O}} + \frac{N_{2} (I_{CM} + 0.5 \Delta i_{CM})}{R_{C} + 0.5 R_{O}}\right) < B_{Sat} A_{O}$$
(12)

The ripple quantities  $\Delta i_{DM}$  and  $\Delta i_{CM}$  in the above inequality can be expressed in terms of  $L_{CM}$  using (3) to (5) or (6) to (8), depending upon the duty cycle the converter. The modified inequality then gives lower bound on the value of  $N_2$ .

D < 0.5

$$N_{2} > \frac{\left(\frac{L_{CM}P_{in}}{4V_{in}} + \frac{V_{in}D(1-2D)}{8(1-D)f}\right)}{\left(B_{Sat}A_{O} - \frac{V_{in}D}{8N_{1}(1-D)f}\right)}$$
(13)

D > 0.5

$$N_{2} > \frac{\binom{L_{CM}P_{in} + V_{in}(2D-1)}{4V_{in}}}{\binom{B_{Sat}A_{O} - \frac{V_{in}}{8N_{o}f}}{}}$$
(14)

A value of  $N_2$  greater than the lower bound defined by the above expressions guarantees the core being unsaturated. The reluctance  $R_C$  can be found by substituting the chosen value of  $N_2$ , satisfying the above inequality constraint, in (8). From  $R_C$ , the airgap length  $l_g$  can be computed using (10). If the computed airgap  $l_g$  is less than desired value,  $N_2$  can be increased such that (13) or (14) is satisfied and the desired airgap is obtained. Large value of  $N_2$  implies wider airgap, which can cause excessive flux fringing and more copper loss.

$$l_g = \frac{R_C \mu_0 \mu_r A_C - l_c}{\mu_r - 1} \tag{10}$$

### V. PROTOTYPE DESIGN AND TESTING

To verify the effectiveness of the proposed structure, a prototype is designed and tested. Table 1 tabulates the prototype converter specifications and required values of  $L_{CM}$  and  $L_{DM}$ . The core used for evaluation is B66375G0500X187 from TDK, with an airgap of 1 mm in the center leg. The core material is N87 ferrite with saturation flux density  $B_{Sat}$  of 490 mT at 25 °C.

TABLE I. PROTOTYPE SPECIFICATIONS

Parameter	Value
$V_{in}$	100 V
$V_{out}$	168 V
$P_{in}$	330 W
f	70 kHz
$\Delta i$	0.670 A
$\Delta i_1 = \Delta i_2$	0.535 A
$L_{CM}$	143 uH
$L_{DM}$	1191 uH

Following the procedure described in the previous section for D < 0.5, the values obtained for the prototype are  $N_1 = 12$ ;  $N_2 = 18$  and  $B_{Lmax} = 142$   $mT < B_{Sat}$ . Fig. 6 shows Finite Element Analysis (FEA) results at the instant where limb flux is maximum in the right outer limb. The maximum magnetic field density is in the 144–144 mT division, which is well below the saturation  $B_{Sat}$  value. The size of the structure can further be reduced by fabricating custom-sized core.

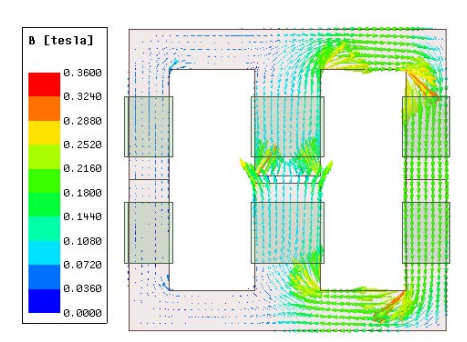


Fig. 6. FEM simulation result for maximum limb flux  $\Phi_{Lmax}$ .

The FEA results are further substantiated by development and testing of the hardware prototype. The developed core with windings is shown in Fig.7. The conductor size selected for the winding is AWG 18. This gives plenty of space for winding and the gap between the core and the windings at the airgap is approximately 36 mm, much greater than the twice of the airgap. Hence, the losses due to fringing at airgap are negligible and can be ignored [10].

TABLE II. TEST RESULTS

Parameter	Value
$V_{in}$	100.5 V
$V_{out}$	168.9 V
$P_{in}$	327 W
f	70 kHz
$\Delta i$	0.574 A
$\Delta i_1 = \Delta i_2$	0.497 A
$L_{CM}$	170 uH
$L_{DM}$	1142 uH

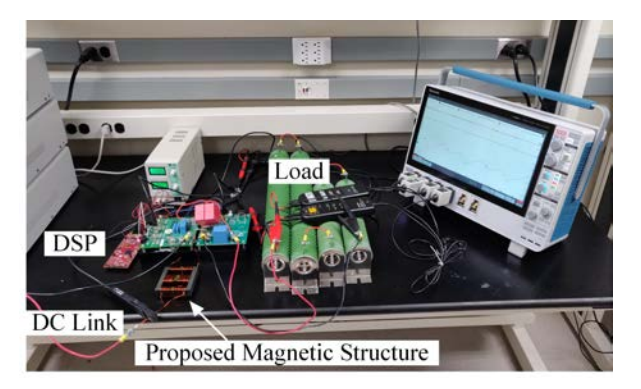


Fig. 7. Experimental setup.

The value of  $L_{CM}$  and  $L_{DM}$ , measured from network analyzer, are 170 uH and 1142 uH respectively. The values differ from the specified values due manufacturing tolerance of the core. As a result, the ripple current values require recalculation using measured values. Plugging in these values in (1) and (2) gives  $\Delta i$  and  $\Delta i_1 = \Delta i_2$  equal to 563 mA and 491 mA for the rated voltage, power, and frequency mentioned in Table I. Fig. 8 shows the experimental setup. For evaluation purpose, two H-Bridge modules KIT8020-CRD-8FF1217P-1 from CREE are as switches. The PWM signals for the switches are generated using Texas Instrument LAUNCHXL-F28379D DSP with duty cycle *D* equal to 0.41. A hardware test is performed, and the measured values are summarized in Table II. The measured values of  $\Delta i$  and  $\Delta i_1 = \Delta i_2$  comes out to be 0.574 A and 0.497 A respectively. The values coincide well with the measured values of  $L_{CM}$  and  $L_{DM}$ . This substantiates the effectiveness of the proposed structure.

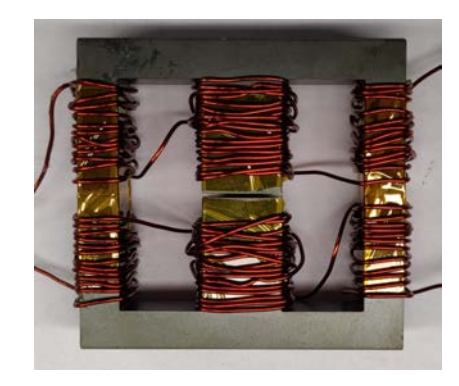


Fig. 8. Prototype developed with  $N_1 = 12$  and  $N_2 = 18$ .

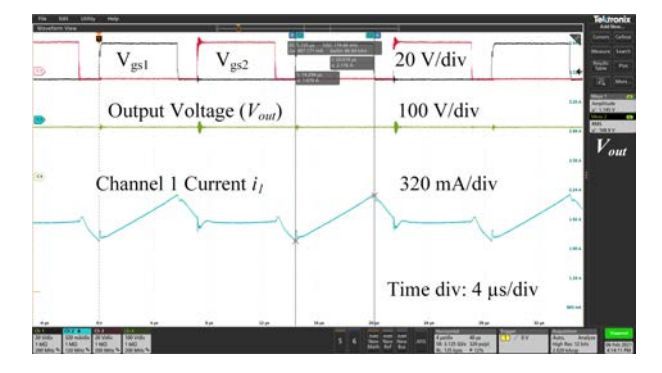


Fig. 9. Experimental Results (Channel Ripple).

### VI. CONCLUSION

Inverse coupled inductor in a two-phase interleaved boost converter can be realized using a cascade of perfectly inverse (DM) and direct (CM) coupled inductors. This approach gives flexibility in obtaining the specified amount of input and channel current ripple. However, the total size of the magnetics is increased. Miniaturization of magnetics can be achieved by combining both CM and DM inductances in a single structure. A gapped EE core-based structure is presented that combines both CM and DM inductances in a single magnetic structure. The CM and DM inductances are independent and depend on different winding turns. A prototype is designed; simulated and tested to validate the proposed concept.

# ACKNOWLEDGMENT

This work was supported by Oak Ridge National Laboratory (ORNL) funded through the Department of Energy (DOE) - Office of Electricity's (OE), Transformer Resilience and Advanced Components (TRAC) program led by the program manager Andre Pereira. The authors would also like to acknowledge the National Science Foundation (NSF Award No. 1846917) for lending financial support for this work.

## REFERENCES

- Wang, C, "Investigation On Interleaved Boost Converters And Applications". Ph.D dissertation. Virginia Polytechnic Institute and State University, Blackburg, 2009.
- [2] M. Muhammad, M. Armstrong and M. A. Elgendy, "A Nonisolated Interleaved Boost Converter for High-Voltage Gain Applications," in *IEEE Journal of Emerging and Selected Topics in Power Electronics*, vol. 4, no. 2, pp. 352-362, June 2016.
- [3] R. Bosshard and J. W. Kolar, "All-SiC 9.5 kW/dm3 On-Board Power Electronics for 50 kW/85 kHz Automotive IPT System," in *IEEE Journal of Emerging and Selected Topics in Power Electronics*, vol. 5, no. 1, pp. 419-431, March 2017.
- [4] J. Imaoka and M. Yamamoto, "A novel integrated magnetic structure suitable for transformer-linked interleaved boost chopper circuit," 2012 IEEE Energy Conversion Congress and Exposition (ECCE), Raleigh, NC, 2012, pp. 3279-3284.
- [5] K. J. Hartnett, J. G. Hayes, M. G. Egan and M. S. Rylko, "CCTT-Core Split-Winding Integrated Magnetic for High-Power DC–DC Converters," in *IEEE Transactions on Power Electronics*, vol. 28, no. 11, pp. 4970-4984, Nov. 2013.
- [6] Pit-Leong Wong, Peng Xu, P. Yang and F. C. Lee, "Performance improvements of interleaving VRMs with coupling inductors," in *IEEE Transactions on Power Electronics*, vol. 16, no. 4, pp. 499-507, July 2001.
- [7] R. Lai, Y. Maillet, F. Wang, S. Wang, R. Burgos and D. Boroyevich, "An Integrated EMI Choke for Differential-Mode and Common-Mode Noise Suppression," in IEEE Transactions on Power Electronics, vol. 25, no. 3, pp. 539-544, March 2010.
- [8] Y. Chu, S. Wang, N. Zhang and D. Fu, "A Common Mode Inductor With External Magnetic Field Immunity, Low-Magnetic Field Emission, and High-Differential Mode Inductance," in *IEEE Transactions on Power Electronics*, vol. 30, no. 12, pp. 6684-6694, Dec. 2015
- [9] H. Zhang, B. Zhang and S. Wang, "Integrated common mode and differential mode inductors with low near magnetic field emission," 2017 IEEE Energy Conversion Congress and Exposition (ECCE), Cincinnati, OH, 2017, pp. 5375-5382.
- [10] S. Jiang, Y. Liu, J. Peng and H. Jiang, "Magnetic Integration of EMI filter for Grid-Connected Voltage-Source Inverters," 2019 10th International Conference on Power Electronics and ECCE Asia (ICPE 2019 - ECCE Asia), Busan, Korea (South), 2019, pp. 917-922.
- [11] Erickson, R. and Dragan, M., 2020. Fundamentals Of Power Electronics. 3rd ed. Springer International Publishing.
- [12] P. Winkler and W. Guenther, "Using Powder Materials to Replace Air-Gaps for Fringing Flux Reduction," PCIM Europe 2017; International

- Exhibition and Conference for Power Electronics, Intelligent Motion, Renewable Energy and Energy Management, Nuremberg, Germany, 2017, pp. 1-6.
- [13] A. I. Emon, B. Narayansamy, H. Peng, Mustafeez-ul-Hassan, Z. Yuan and F. Luo, "Investigation of Power Converter's Near Field EMI Containment Using Passive Filters," 2020 IEEE International Symposium on Electromagnetic Compatibility & Signal/Power Integrity (EMCSI), 2020, pp. 398-403.